

## **General Disclaimer**

### **One or more of the Following Statements may affect this Document**

- This document has been reproduced from the best copy furnished by the organizational source. It is being released in the interest of making available as much information as possible.
- This document may contain data, which exceeds the sheet parameters. It was furnished in this condition by the organizational source and is the best copy available.
- This document may contain tone-on-tone or color graphs, charts and/or pictures, which have been reproduced in black and white.
- This document is paginated as submitted by the original source.
- Portions of this document are not fully legible due to the historical nature of some of the material. However, it is the best reproduction available from the original submission.

# PARTS AND COMPONENTS EVALUATION REPORT

DRA



PACER #08-005  
June 19, 1974

CHANGES IN THE PERFORMANCE CHARACTERISTICS OF

A GaAs NEAR INFRARED LIGHT EMITTING DIODE

WHEN EXPOSED TO VARIOUS CURRENT AND THERMAL STRESSES

(NASA-TM-X-72596) CHANGES IN THE  
PERFORMANCE CHARACTERISTICS OF A GaAs NEAR  
INFRARED LIGHT EMITTING DIODE WHEN EXPOSED  
TO VARIOUS CURRENT AND THERMAL STRESSES

(NASA) 43 HC \$4.00

N76-20997

Unclass  
17361

CSCL 20L G3/76



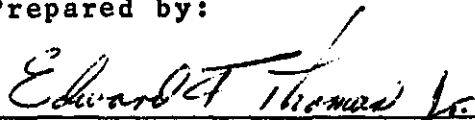
FAILURE ANALYSIS SECTION  
QUALITY ASSURANCE DIVISION  
GODDARD SPACE FLIGHT CENTER

CHANGES IN THE PERFORMANCE CHARACTERISTICS OF  
A GaAs NEAR INFRARED LIGHT EMITTING DIODE  
WHEN EXPOSED TO VARIOUS CURRENT AND THERMAL STRESSES

by

Edward F. Thomas, Jr.

Prepared by:



Edward F. Thomas, Jr.  
Failure Analysis Section  
Parts Branch, QAD

Approved by:



William J. Kneval  
Head, Parts Branch, QAD

"The information contained herein is presented for guidance of employees of the Goddard Space Flight Center. It may be altered, revised or rescinded due to subsequent developments or additional test results. These changes could be communicated internally by other Goddard publications.

"Notice is hereby given that this document is distributed outside of Goddard as a courtesy only to other Government agencies and contractors and is understood to be only advisory in nature.

"Neither the United States Government nor any person acting on behalf of the United States Government assumes any liability resulting from the use of the information contained herein."

**ORIGINAL PAGE IS  
OF POOR QUALITY**

#### ACKNOWLEDGEMENT

I wish to express my appreciation and sincere thanks to Mr. Samuel Floyd, who conducted the thermal stress test cells of this program, and who helped considerably in formulating the ideas and concepts that comprise this report.

## I. SUMMARY

This report discusses the changes that occurred in the optical and electrical characteristics of a near infrared, GaAs light emitting diode (LED), when operated under various levels and combinations of current and thermal stresses. A total of forty parts were operated for two thousand hours under eight different sets of dc current and ambient temperature conditions. Degradation in the radiant optical power of these devices was thirty-four percent when operated at their rated current and an ambient temperature of 298K (25°C). Derating the current and/or the thermal stress reduced the degradation of this parameter in approximately a linear manner. In fact, parts operated at twenty-five percent of the rated current value exhibited negligible degradation. All degraded devices behaved similarly, exhibiting rapid non-linear degradation followed by a gradual linear degradation and finally a period of stable operation.

An attempt was made to correlate initial device condition (both optical and electrical) to degradation during stress testing, but met with little success. However, it appeared that those devices having the higher initial radiant optical power values exhibited smaller amounts of degradation of that parameter when stressed at the various current levels.

Of the forty devices tested, (five of them above rated current), only one catastrophic failure occurred. This device was operated at twenty-five percent above the rated current stress of two hundred milliamperes and an ambient temperature of 298K (25°C), and failed after operating for six hundred and twenty-five hours. This device initially had non-typical I-V characteristics (high forward and reverse leakage currents) and it is believed that this factor, combined with the high current stress, caused the events that ended in catastrophic failure.

## II. INTRODUCTION

### 1. Background

As the technology for producing light emitting diodes continues to improve, more and more of these devices are being used in applications that require high reliability parts. Although, theoretically, these devices should operate for extended periods of time with little or no degradation, experience has shown that they do undergo degradation that can, at times, be quite severe.

The objective of this program was twofold, first to determine the performance or degradation characteristics of a light emitting diode under the most commonly experienced stresses, current and temperature; and then, based on this information, to define methods for determining if the inherent capabilities of these parts are compatible with intended applications.

### 2. Parts Description

#### a. Physical Characteristics

The light emitting diode selected for use in this test program was the TIL-31, manufactured by Texas Instruments, Incorporated of Dallas, Texas. The TIL-31 consists of a solution grown GaAs chip (approximately  $3.75 \times 10^{-2}$  cm on a side) eutectically bonded to a conventional TO-46 transistor header, and covered by an epoxy dome. The epoxy dome increases the amount of light leaving the chip surface by increasing the angle of internal reflection of the GaAs. The top of the TO-46 can contains a lens which provides for some focusing of the output beam. Figure 1 details the internal construction of the TIL-31.

The GaAs chip used in this device is doped with silicon to form the necessary P-N junction required for proper operation of the LED. Electrical connection is made to the top surface of the chip by attaching a gold wire to a metallized gold-germanium area, using a thermocompression ball bond.

#### b. Optical Characteristics

The TIL-31 emits energy in the near infrared portion of the spectrum with a peak wavelength ( $\lambda_p$ ) of  $0.94 \mu\text{m}$  and a spectral band width between half-power points ( $BW_\lambda$ ) of  $600 \text{ \AA}$ . The specified minimum total radiant optical power ( $P_o$ ), measured at a forward dc current of 100 mA, is 3.3 milliwatts. The rise and fall times of this optical output are relatively fast, approximately 300 to 600 ns.

c. Electrical Characteris

Because the TIL-31 is essentially a P-N junction diode, it possesses normal forward and reverse diode characteristics. Unlike silicon diodes, however, that have a junction barrier potential of 0.6 to 0.7 volts, the GaAs device has a junction barrier potential of approximately 1.0 volt. The reverse I-V characteristics for these devices are generally sharp, with breakdown voltages varying from two to forty volts. The reverse leakage currents are, in most devices, extremely low,  $10^{-11}$  to  $10^{-12}$  amperes.

III. APPROACH

1. Stress Test Matrix

In light emitting diodes, forward biasing is required for the generation of light. Furthermore, the amount of light produced is directly proportional to the forward current. Unfortunately, degradation in these devices also occurs under forward biasing. In order to arrive at an effective compromise between degradation and optical output, the performance characteristics of these devices must be defined for various levels of forward current operation. In addition, since all semiconductor devices are adversely affected by increased chip temperatures, this additional variable should be considered as a factor in determining device performance.

In order to determine the combined influence of these two stress variables (current and temperature), the matrix test of Table I was developed.

TABLE I. CURRENT AND THERMAL STRESS TEST MATRIX

		Ambient Temperature - K			
		298	323	348	373
Current Stress - mA	50				
	100				
	200				
	250				

Shaded Cells Were Test Cells



By subjecting devices to the conditions indicated for the shaded cells, degradation resulting from the individual and combined stresses can be evaluated. The test devices were exposed to the conditions of each test cell for a period of two thousand hours.

## 2. Parameter Measurements

### a. Optical

The basic parameter for a light emitting diode is radiant optical power ( $P_o$ ). As was mentioned previously, total emitted  $P_o$  is specified by the manufacturer to be a minimum of 3.3 milliwatts when measured at a dc current of 100 mA. This parameter is, for the most part, a linear function of forward current. Therefore, since the TIL-31 is rated for a current of 200 mA, it is capable of emitting at this current, a minimum of 6.6 milliwatts of total optical power.

The amount of total emitted optical power that can be used in any specific application depends upon the pattern of the emitted energy, the size and geometry of the detecting element, and the spacing between the emitter and detector. In order to define the radiated beam pattern of the TIL-31, an infrared photograph was taken of the output at a fixed distance of 0.7 cm. This separation was determined by the instrumentation used to measure optical output. The beam pattern obtained was 2.2 cm in diameter and is shown in Figure 2(a). The area irradiated by the beam, at this relatively close spacing of 0.7 cm, is large ( $3.8 \text{ cm}^2$ ). It should also be noted that the intensity of the radiated energy is not uniform over this area, but rather varies as is shown in the intensity profile plot of Figure 2(b).

Usually, the TIL-31 light emitting diode is used in conjunction with a companion sensor, the TIL-81 silicon photo-transistor, a device that responds favorably to the output power level and wavelength of this source. Physically, the TIL-81 is encased in a TO-18 transistor package and has a glass window in the top of the can. This window is 0.47 cm in diameter, offering a receptive surface area of  $0.173 \text{ cm}^2$ . Comparing this receptive area to the total area irradiated by the TIL-31 emitter at a distance of 0.7 cm ( $3.8 \text{ cm}^2$ ), illustrates that this sensor does not utilize the total radiated energy of the TIL-31.

Because of this situation, it was considered more meaningful for testing purposes, to define a new parameter for the TIL-31 light emitting diode. This new parameter, usable radiant optical power ( $P_o'$ ), is defined as the amount of radiated optical power that would be intercepted by the TIL-81 sensor, or a detector element of equivalent receptive surface area. All measurements of  $P_o$  noted in this report were made at 100 mA using an equivalent surface area detector, a thermopile element having a receptive area of  $0.184 \text{ cm}^2$ . A discussion of various methods for measuring  $P_o$ , detecting surfaces that can be used, the rationale for using a thermopile element for this investigation, and a description of the specific instrumentation used in this program is presented in Appendix A of this report.

Seventy-three TIL-31 devices were procured for this program and were all date coded 215, indicating that the packages were tested during the fifteenth week of 1972. The usable radiant optical power ( $P_o'$ ) of each device was measured over the range of current values from  $3.0 \times 10^{-4}$  to  $2.0 \times 10^{-1}$  amperes. Figure 3 shows the distribution of values of  $P_o'$  measured at 100 mA for all seventy-three parts. Measured values of  $P_o'$  ranged from 0.26 milliwatts to 1.15 milliwatts, with an average value of 0.76 milliwatts. Figure 4 is a representative plot of  $P_o'$  as a function of forward current, and shows the linear relationship mentioned earlier. All measurements of  $P_o'$  mentioned in this report were made at a distance 0.7 cm in front of the emitter for reasons stated earlier. The plot of Figure 5 shows how the value of  $P_o'$  varies as emitter to detector separation increases beyond the 0.7 cm separation.

In addition to the measurement of  $P_o'$ , measurements were made of the wavelength of peak emission ( $\lambda_p$ ) and spectral band-width ( $BW_\lambda$ ). Figure 6 shows a typical spectral response curve of radiant intensity as a function of wavelength. All wavelength measurements were made using a 0.25m Ebert monochromator. Distributions of the values of  $\lambda_p$  and  $BW_\lambda$  for the procured sample, measured at a current of 100 mA, are shown in Figure 7.

#### b. Electrical

Since the light emitting diode is basically a P-N junction diode, the electrical parameters measure forward and reverse junction characteristics. The forward and reverse junction currents of each device were measured over the voltage range of 0.1 to 1.4 volts. A typical plot of these parameters is shown in Figure 8. The forward current, when plotted on semi-logarithmic graph paper as a function of forward voltage, is a straight line, until the diode series

resistance becomes appreciable, at which point the current begins to saturate. The reverse current plot is similar to that for a silicon junction diode except that the current levels are lower for the GaAs diode,  $10^{-11}$  to  $10^{-12}$  amperes, as compared with  $10^{-7}$  to  $10^{-8}$  amperes for a silicon device.

In addition to the current measurements, the reverse breakdown voltage of each device was measured and a notation made as to whether the reverse characteristic was sharp, indicating a properly made junction, or soft, indicating some type of abnormality. Of the seventy-three parts so measured, sixteen or twenty-two percent exhibited a soft or unusual reverse I-V characteristic. Figure 9 shows the distribution of breakdown voltages for the procured sample. Because of the concentration of devices having breakdown voltage values around 7 to 8 volts and around 40 to 42 volts, it may be that this one date code lot of devices contains more than one diffusion lot, thereby producing more than one grouping of breakdown voltage values.

#### c. Electrical/Optical Correlation

An effort was made to find a correlation between initial electrical and optical parameters, but did not meet with much success. An analysis of the data indicated that there may be a degree of correlation between reverse breakdown voltage and  $\lambda_p$ , with devices having low reverse breakdown voltage readings also exhibiting high values of  $\lambda_p$  and vice versa. However, because of the small sampling, the possibility that the sampling represents more than one diffusion lot, and the difficulty of making extremely accurate  $\lambda_p$  measurements, more data would be required to confirm or deny this relationship.

### 3. Device Classification

Each device in the procured lot was assigned classifications according to its initial electrical and optical measurement values. In order to assure that a representative group of devices were included in each of the operated stress matrix cells, and to facilitate the task of determining whether or not initial electrical and/or optical measured values related to device degradation under stress, devices from each classification group were selected to fill each test cell. The electrical classification was based on the shape of the junction I-V characteristics, while the optical classification was based on the magnitude of the initial value of  $P_o'$ . Table II lists the classification codes and the criteria determining the classification assignment.

TABLE II. LED CLASSIFICATION CODE AND CRITERIA

Code	Classification Criteria
$D_f$	Non-typical forward I-V characteristic
$D_R$	Non-typical reverse I-V characteristic
A	$P_o' > 0.93$ milliwatts
B	$0.59 \leq P_o' \leq 0.93$ milliwatts
C	$P_o' < 0.59$ milliwatts

A detailed explanation for the derivation and rationale of the classification criteria is presented in Appendix B.

#### IV. INVESTIGATION AND RESULTS

##### 1. Optical Degradation

Usable radiant optical power ( $P_o'$ ) was measured periodically throughout the stress testing. In nearly all devices under test, there was an increase in  $P_o'$  very early in the stress testing, the magnitude and time rate of change of which was a function of the stress level. Devices operated at the highest current stress of two hundred and fifty milliamperes exhibited increases in  $P_o'$  of ten percent while those operated at the lower current stresses exhibited increases ranging from two to five percent. At the highest current stress, only fifty hours was required for devices to reach their peak value of  $P_o'$  while at the lower current stresses, two hundred hours were required. This phenomena of initial increase in  $P_o'$  has been noted by other investigators, and it is my opinion that this increase is caused by the annealing of the materials used in fabricating the diode chip; or, in other words, the release of built in stresses resulting from the fabrication process.

After all increases in  $P_o'$  ceased, degradation of this parameter became evident. The percentage of degradation, occurring at any point in time after full annealing, was based on the peak or fully annealed value of  $P_o'$ . Figures 10 and 11 show the average degradation of  $P_o'$  that occurred as a result of

the current and thermal stress tests over a period of two thousand hours. These curves show that current stress had by far the greater effect on  $P_o'$ .

The shape of the degradation curves is extremely interesting for two reasons. First, it appears that there exists, for this device, a single characteristic degradation curve for both current and thermal stress, the shape of which is best defined by the two highest current stress plots. Initially, degradation was non-linear and quite rapid. This was followed by a region of gradual, linear degradation, and finally a region of stability. The specific characteristics of each of these three regions was related to the level of stress.

The second factor of interest involves the region of stability. From this one can conclude that it may be possible to stabilize this type of part by means of a short term/high stress burn-in test. After stabilization, it may be possible to operate parts at a derated current level without further degradation of  $P_o'$ . The trade off here would be increased stability of  $P_o'$  for an initially lower optical output.

A Summary of the degradation of  $P_o'$  after two thousand hours is given in Table III.

TABLE III. Radiant Optical Power Degradation  
After Two Thousand Hours of Operation

Stress	$P_o'$ (Ave.)	Range of $P_o'$ (5 parts)
50 MA, 298K (25°C)	3.2%	0 - 6.5%
50 MA, 323K (50°C)	9.1%	3.1 - 13.2%
50 MA, 348K (75°C)	11.6%	2.5 - 20.7%
50 MA, 373K (100°C)	16.6%	4.9 - 28.2%
100 MA, 298K (25°C)	14.5%	0 - 28.9%
100 MA, 323K (50°C)	20.9%	13.3 - 39.4%
200 MA, 298K (25°C)	35.1%	31.5 - 37.8%
250 MA, 298K (25°C)	43.0%	39.1 - 47.1% *

\* Based on four parts due to one catastrophic failure.

From Table III it can be seen that some test groups exhibited very small ranges of  $P_o'$  values, while other groups exhibited fairly large ranges of  $P_o'$  values. Two factors that affect the variance observed between devices operated at the same level are the optical measurement sensitivity and annealing. These factors and their effect on the measured degradation of radiant power output are discussed in Appendix C of this report.

By plotting the average degradation values of  $P_o'$  from Table III, the individual effects of current and temperature stress can be determined. These plots show that the degradation of  $P_o'$  resulting from two thousand hours of operation is a linear function of both the current stress at constant ambient temperature (Figure 12a) and the temperature stress at constant current (Figure 12b). Plotting degradation of  $P_o'$  as a function of combined current and thermal stresses results in a third linear plot (Figure 12c). Using this third plot, an estimate can be made of the degradation that would occur within two thousand hours of operation for a large variety of driving currents and ambient temperatures.

It was mentioned earlier that each stress group contained parts having different classifications based on initial optical and electrical characteristics. No correlation was found to exist between the degradation of  $P_o'$  and the initial condition of the device I-V characteristics. Devices having non-typical I-V characteristics did not exhibit unusual degradation of  $P_o'$ . There was, however, a slight correlation between the initial value of  $P_o'$  and the amount of degradation occurring in that parameter with time and stress. Especially in the lower stress groups, those devices having initially higher values of  $P_o'$  exhibited lower total degradation after two thousand hours of operation.

The optical parameters measured in addition to the radiant power were the wavelength of peak emission ( $\lambda_p$ ) and the spectral bandwidth ( $BW_\lambda$ ). Neither parameter changed significantly during two thousand hours of operation. Based upon the measurement of control devices, the sensitivity of the  $\lambda_p$  measurement was found to be on the average  $\pm 0.4\%$  ( $\pm 40 \text{ \AA}$ ). Similarly, the sensitivity of the  $BW_\lambda$  measurement was found to be  $\pm 8\%$  ( $\pm 50 \text{ \AA}$ ). Although all  $\lambda_p$  and  $BW_\lambda$  values measured after the start of stress testing were lower than the initial measured values, the percentage change in every case was within the observed measurement sensitivities. It can be stated then that no changes greater than  $\pm 0.4\%$  for the  $\lambda_p$  parameter and  $\pm 8\%$  for the  $BW_\lambda$  parameter occurred as a result of exposure of the devices to stress, but that there was overwhelming evidence that the values of both parameters did decrease slightly during test.

## 2. Electrical Degradation

The only changes occurring in the forward I-V characteristics of these parts occurred in the lower current region below a forward junction potential of approximately 0.9 volts. The forward I-V characteristics for one part stressed at two hundred and fifty milliamperes is presented in Figure 13 as a typical example of this change. Conversely to this, very large changes occurred in the reverse I-V characteristics as is evidenced by the plots of Figure 14 which show the increase in reverse leakage current as a function of current stress and time. At the two hundred and two hundred and fifty milliamperes current levels, the reverse leakage currents measured at 1.4 volts increased by a factor of ten thousand, with the bulk of the change occurring within the first few hundred hours. At a current stress of one hundred milliamperes, after two thousand hours, the reverse leakage current had increased by a factor of two hundred. At the lowest current stress of fifty milliamperes, there was only a factor of ten increase.

Devices classified as having non-typical forward and/or reverse I-V characteristics did not degrade differently from those devices having typical I-V characteristics. Since  $D_R$  devices did have initially larger leakage currents, degraded current levels for these devices were quite high, with the highest value recorded at 1.4V being  $1.5 \times 10^{-5}$  amperes. There was one exception to the general statement made above, namely that one device failed catastrophically and that this device had a non-typical forward and reverse characteristic initially. This particular part will be discussed in more detail later in this report.

Initially, most devices, when examined on a curve tracer to determine the reverse breakdown characteristics, exhibited normal characteristics; that is, relatively high and sharp breakdown voltages. After stress, particularly in the two highest current stress groups where it occurred in all devices, the reverse characteristics became soft. So severe was this condition in many devices, that breakdown voltage values could not be measured due to the high reverse leakage currents. The problem with degradation of the reverse characteristic is not that it relates to the degradation of radiant optical power (no such correlation was found) but that if reverse voltages greater than a couple of volts appear momentarily across the device during use, catastrophic failure due to electrical overstress might occur.

### 3. Catastrophic Failure

One catastrophic failure occurred during the two thousand hours of testing. This device was operated at a current stress of two hundred and fifty milliamperes (twenty-five percent above manufacturer rated conditions) and an ambient temperature of 298K (25°C). The part failed electrically open after six hundred and twenty-five hours of operation. Figure 15 is a plot of the degradation of  $P_o'$  for this device up until the time of failure. For comparison purposes, the average response curve for this stress level is included to show the deviation in the  $P_o'$  degradation of the failed device.

Figure 16 is a plot of the forward I-V characteristic both initially and after five hundred hours of operation. It can be seen that significant changes occurred in this characteristic. The forward current values below the junction potential voltage of 1.0 volts were increased after the exposure to stress, but not in a manner greatly different than that of the other devices exposed to the two highest current stress levels (see Figure 14). However, whereas the forward current values above this voltage did not change appreciably over the initial values for devices in these stress groups, the device that failed catastrophically underwent a large reduction in forward current values above the junction potential voltage. The immediate result of this change in the forward characteristic, since these devices were all operated at constant forward current stress, was a significant increase in electrical power dissipation, which increased junction temperature. Degradation of the reverse I-V characteristic for this device was not significantly different from that of other devices in the same stress group. Therefore, it is concluded that the significant changes occurring in this device involved the forward conduction process.

Upon electrically examining the catastrophically failed device, it was confirmed that there existed an electrical open circuit within the part. Decapping this part revealed severe discoloration of the epoxy dome, so severe in fact that the chip and wire bond could not be visually inspected through the epoxy. After potting this specimen and grinding down through the top of the dome, a point was reached where the chip and wire bond could be observed. Figure 17 is a photograph of this view. It was observed that the excessively high chip temperature decomposed the epoxy immediately above the chip surface, and resulted in the interconnect gold wire melting open.



What apparently occurred in this device was an increase in forward resistance which caused both a reduction in the forward current at a specific voltage and an increase in the power dissipation at a fixed current stress of two hundred and fifty milliamperes. The resulting increase in chip temperature both accelerated this condition and also discolored and finally decomposed the epoxy in the immediate vicinity of the chip. Final failure occurred when sufficient temperature was generated to melt open the gold interconnect wire bonded to the chip surface. The extremely large decrease in  $P_o'$  noted in Figure 15 was most likely due to a combination of factors, first a reduction in the magnitude of the light producing current component from the total forward current because of the increase in forward resistance, and second the discoloration and near opaqueness of the epoxy dome itself. The initial classification of this device identified it as a poor emitter of radiant optical power (class C) and as having a non-typical forward I-V characteristic ( $D_f$ ). It is believed that the non-typical forward characteristic combined with the high current stress led to the causes listed above, which culminated in total failure after six hundred and twenty-five hours of operation.

## V. CONCLUSIONS AND RECOMMENDATIONS

It was observed that degradation of usable radiant power output ( $P_o'$ ) occurred under all current stress levels. However, at the lowest stress, only three percent was measured. Although these devices are rated for use at a drive current of two hundred milliamperes, degradation at this stress was observed to be large, 34.5% in two thousand hours of operation. If an application requirement was such that this amount of degradation could not be tolerated, these devices would have to be derated (i.e. operated at below rated current levels). It must be realized that although a reduction in drive current will result in less degradation of  $P_o'$ , it also will result in less  $P_o'$  emitted. Therefore, the lower level of  $P_o'$  would have to be acceptable or another part type selected.

Infrared photographs of the TIL-31 output beam pattern and measurements of  $P_o$  using a  $0.184 \text{ cm}^2$  receptive area detector element have shown that there can be large differences between the total amount of  $P_o$  that is emitted, and the portion that is available for use in specific applications. If a system design is based upon total emitted  $P_o$  while in fact usable  $P_o$  is much less, a problem will result. Larger than planned drive currents will be required to obtain the desired

levels of usable  $P_o$ , thereby increasing degradation of this parameter. It is possible to maximize  $P_o'$  for any given current by selecting parts having the highest initial values of  $P_o'$ , keeping the source to detector separation as small as possible, and by providing the potential for peaking usable power by means of centering the detector element within the emitted beam pattern. It is recommended that for both system design purposes and part selection, usable radiant power measurements be made a requirement.

For applications requiring an extremely stable output, it may be possible to stabilize parts by subjecting them to a short term/high stress burn-in. Once stabilized at the high stress level, it may be possible to operate the parts at a current level below the burn-in level without further degradation. The trade off in achieving this would be lower  $P_o'$  values at the operated current level as a result of the burn-in test. additional work needs to be performed to verify if such stabilization of  $P_o'$  could be achieved.

Although these devices are operated in the forward conducting mode, it is a possibility that negative voltages could appear across the device during operation. Because of the softening of the reverse I-V characteristics and large increases in reverse leakage currents observed during these stress tests, this situation could result in catastrophic failure depending upon the magnitude of the reverse voltage stress and the degree of degradation in the reverse I-V characteristics. Therefore, it is recommended that reverse voltages should not be applied to these parts during operation.

Finally, although one device tested failed catastrophically during operation, the operated stress level, initial condition of the device, and the successful operation of other devices at equivalent stress levels for two thousand hours indicate that the failure was related to the non-typical forward I-V characteristic, and that similar failures would not likely occur at rated or derated current levels, providing that devices with non-typical forward characteristics were removed by electrical testing.

## APPENDIX A

### OPTICAL MEASUREMENTS OF NEAR INFRARED LIGHT EMITTING DIODES

The manufacturer of the TIL-31 near infrared light emitting diode measures and specifies a total radiant optical output of this device ( $P_o$ ) when measured at a dc current of 100 mA. The technique used in making this measurement is to completely surround the emitter with several detector surfaces, summing the response of all detectors to obtain total radiated power. Similar results using a single detector surface could be obtained providing the surface area was large enough to receive the total beam of radiated energy. Another technique for measuring total radiant energy with a single detector surface would be to use a light pipe for coupling the emitted energy directly to the detector surface. The advantages of using a light pipe are that it would permit the use of a relatively small detector surface, and also provide thermal isolation between the emitter and detector. Losses will occur however during the transmission of radiant energy, and it would be necessary to measure and correct for these losses.

Although the measurement of total radiant energy does allow one to determine the full capability of the emitter, this measurement has limited use in system design. In most applications, only a portion of the total power emitted is received and utilized. Therefore, it is essential that radiant power levels used in design be usable power levels for that application. Since the amount of usable power will, in general, vary with the application, a general definition of this parameter was developed for use in this test program. As used here, usable radiant power ( $P_o'$ ) is defined as that amount of radiant power that is intercepted by a TIL-81 silicon photo-transistor, the companion sensor to the TIL-31, or a detector element of equivalent receptive surface area.

There are several types of detectors that can be used to measure the radiant optical power of the TIL-31 near infrared light emitting diode. These are silicon detectors, photo-multiplier tubes and thermopiles. Since each type of detector offers certain advantages and disadvantages, the specific requirements of the measurement will more or less dictate the selection of the type detector to be used. The test program for which these radiant power measurements were to be made has, as its purpose, the determination of the degradation of this

parameter with time. Therefore, many measurements would be necessary extending over a long period of time. To accomplish the program objective then, the measurements of radiant optical power would have to be repeatable. In addition, because of the large number of measurements that would be required, it is imperative that these measurements be quickly and easily made. In addition, since there might be additional follow-on programs involving different types of optoelectronic devices, the instrument selected should be versatile, and able to handle the large variety of parts available today.

Silicon detectors have the basic advantage that they are inexpensive, sturdy, relatively stable, and have a wide spectral response. These detectors, however, are not extremely sensitive and, because their spectral response curve is non-linear, the measurements obtained must be altered depending upon the wavelengths being radiated. This latter fact complicates the measurement procedure and requires that the wavelength of the radiant energy be known precisely, both initially and as a function of time.

Photomultiplier tubes are extremely sensitive and have a moderate spectral response. These detectors however, require large power supplies, are expensive, bulky and are susceptible to instabilities arising both in the power supply and in the photomultiplier tube itself. Also, as with the silicon detectors these devices have a non-linear spectral response curve which complicates the measurement and interpretation of the radiant optical power of various optoelectronic devices.

Thermopile detectors have a very wide range, flat spectral response curve, moderate sensitivity and are relatively small and inexpensive. Because they are thermal devices, however, they are susceptible to temperature variations, require short stabilization periods between measurements, and have relative slow response times. Since most of the above disadvantages of the thermopile detector can be minimized with proper design, and because the ease of making and interpreting measurements is unaffected by wavelength, the thermopile detector was selected as the means for making the radiant power measurements in this program. Other positive factors resulting from this selection were its versatility, based on the wide range, flat spectral response curve, and its low cost.

The instrument used for the radiant power output measurements was the Hewlett-Packard Model 8330/8334A Flux Meter/Detector. The thermopile detector portion of this instrument consists of sixty-four individual bismuth-antimony thermocouples arranged in a 8x8 matrix, 0.428 cm x 0.430 cm. As was anticipated, the design of this particular detector resulted in the minimization of the deleterious effects of thermal instability, sensitivity, and slow response time. Since the receptive surface area of this thermopile detector element closely matches the receptive surface area of the TIL-81 sensor (within 6%) measurements of  $P_o$  are interpreted as being measurements of  $P_o'$  as defined in this report.

To facilitate the measurement of  $P_o'$  and maintain a fixed source to detector separation of 0.7 cm, special holding fixtures were designed and fabricated. Figure 18 shows the test fixtures, instrumentation and measurement configurations for making the optical radiant power output measurements discussed in this report. Figure 19 shows the setup and instrumentation for making the wavelength of peak emission ( $\lambda_p$ ) and the spectral bandwidth measurements ( $BW_\lambda$ ).

## APPENDIX B

### THE CLASSIFICATION OF TIL-31 LIGHT EMITTING DIODES ACCORDING TO INITIAL ELECTRICAL AND OPTICAL PARAMETER VALUES

The classification criteria pertaining to the initial electrical measurements was based on the shape of the junction I-V characteristics. If forward junction current is plotted against forward voltage on semi-logarithmic graph paper, a linear relationship will exist up until the point where diode series resistance becomes appreciable. At this point forward current begins to saturate. Devices that did not show this general type of forward I-V characteristic were classified as  $D_f$ , indicating that they possessed a non-typical forward characteristic. A similar rationale was applied to the reverse junction characteristics in that those devices that did not exhibit a typical reverse characteristic were classified as  $D_R$ . Examples of typical and non-typical junction characteristics are presented in Figure 20.

The optical classification was based on the initial measured value of  $P_o'$ . From the distribution of the measured values, it was determined that the mean value was 0.76 milliwatts, and that the standard deviation of this sampling was 0.17 milliwatts. Therefore, high  $P_o'$  devices, those having values greater than the mean value plus one standard deviation (0.93 milliwatts) were identified as being class A parts. Conversely, low  $P_o'$  devices, those having values less than the mean value minus one standard deviation (0.59 milliwatts) were identified as being class C devices. All other medium  $P_o'$  devices were identified as being class B parts.

It follows from the above discussion that since the electrical and optical classifications are exclusive of one another all devices classified as  $D_f$  or  $D_R$  also have an optical, A, B or C classification.

## APPENDIX C

### VARIATIONS IN THE DEGRADATION OF $P_o'$

There are two sources for observed variation in the degradation of  $P_o'$  between devices operated under the same stress conditions. First, annealing occurs in these devices very early in the stress testing, and results in an increase in  $P_o'$ . This increase is a function of stress. However, of more importance is the fact that the increase of  $P_o'$  is also highly individualistic, since the magnitude of the increase is also a function of the degree of built-in stresses resulting from the fabrication process. This obviously can vary from device to device.

Evidence of this fact comes from measurements of devices that were not subjected to current or thermal stresses, but that had only undergone room temperature storage for seven thousand hours. After this period of time, a total of twelve unstressed parts were resubmitted for  $P_o'$  measurements. All twelve devices exhibited an increase in  $P_o'$  ranging from 2.0 to 22.5%, with an average increase of 11%. This large variation points out the potential difference existing between devices. It is also interesting to note that the average increase of 11% compares very well with the increase observed during the highest current stress exposure, namely 10%.

The second source of observed variation is measurement uncertainty. Values of  $P_o'$  were measured to an accuracy of  $\pm 0.02$  milliwatts. This meant that the measurement error was on the average  $\pm 2.6\%$ , but actually ranged from  $\pm 1.8\%$  to  $\pm 6.7\%$  depending upon the magnitude of  $P_o'$  being measured.

Therefore, because of measurement uncertainty, variations as large as 6 or 7% could be expected. Three of the eight stress groups showed variations of this order. The remaining groups showed variations of 28%. The additional effects of annealing as described above, would be sufficient to account for this larger level of variability.

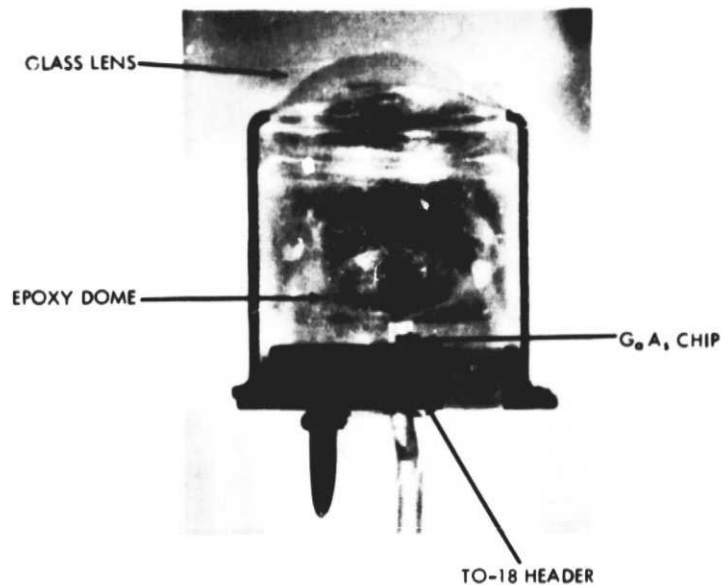
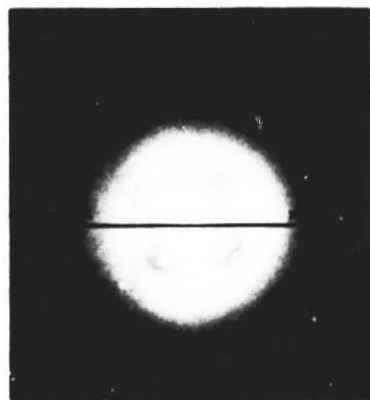
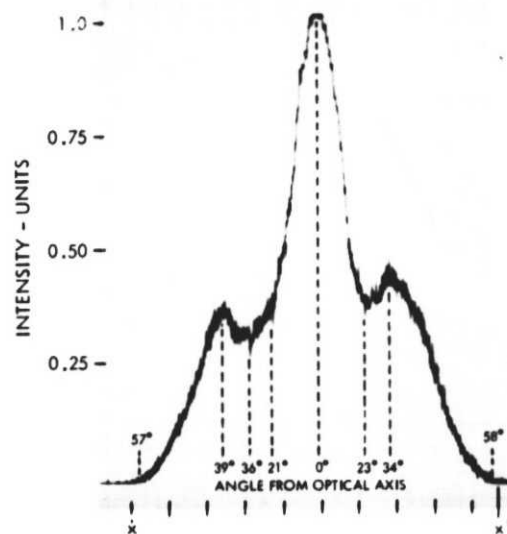


Figure 1. Internal Construction of the TIL-31, Infrared LED  
(12 X Mag)



2(a) IR Photograph of the Optical Output of the  
TIL-31 (2X MAG.)



2(b) Intensity Profile of a Scan Across the Center of the  
TIL-31 Beam Pattern (3.5X MAG)

Figure 2 Optical Output Beam Pattern for the TIL-31 at a Distance of 0.7 cm

**PRECEDING PAGE BLANK NOT FILMED**



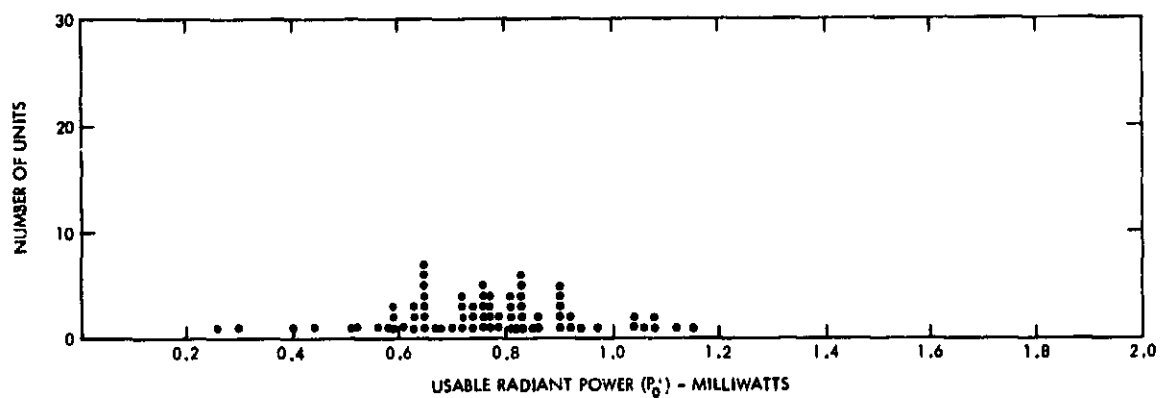


Figure 3. Distribution Of Initial Values Of Usable Radiant Power ( $P_0'$ ) Measured At 100 Milliamperes

ORIGINAL PAGE IS  
OF POOR QUALITY

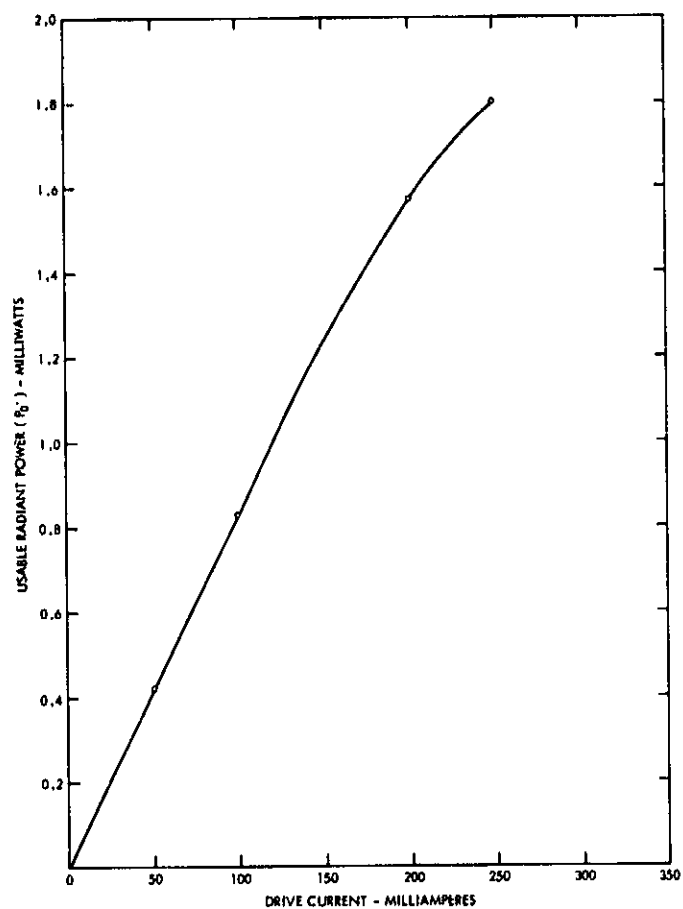


Figure 4. A Typical Plot Of Usable Radiant Power As A Function Of Drive Current For A Separation Of 0.7 cm .

ORIGINAL PAGE IS  
OF POOR QUALITY

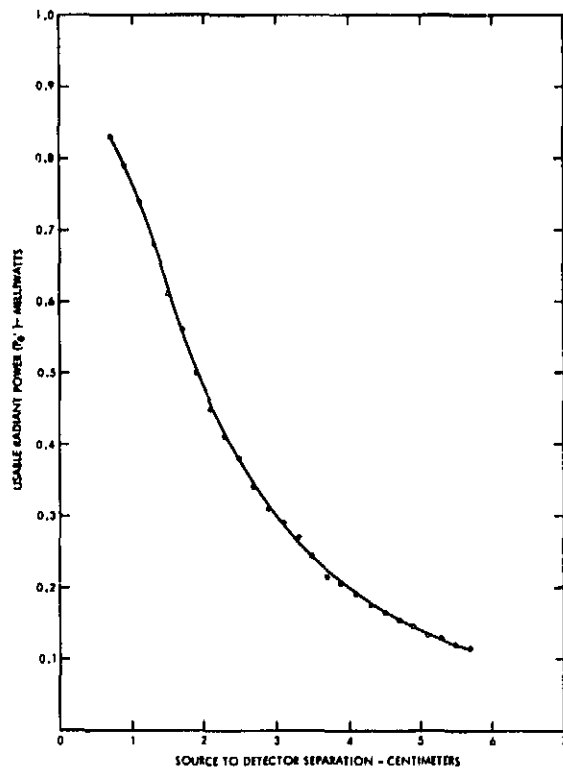


Figure 5. Usable Radiant Power ( $P_u$ ) As A Function Of Source To Detector Separation For A Drive Current Of 100 Milliamperes

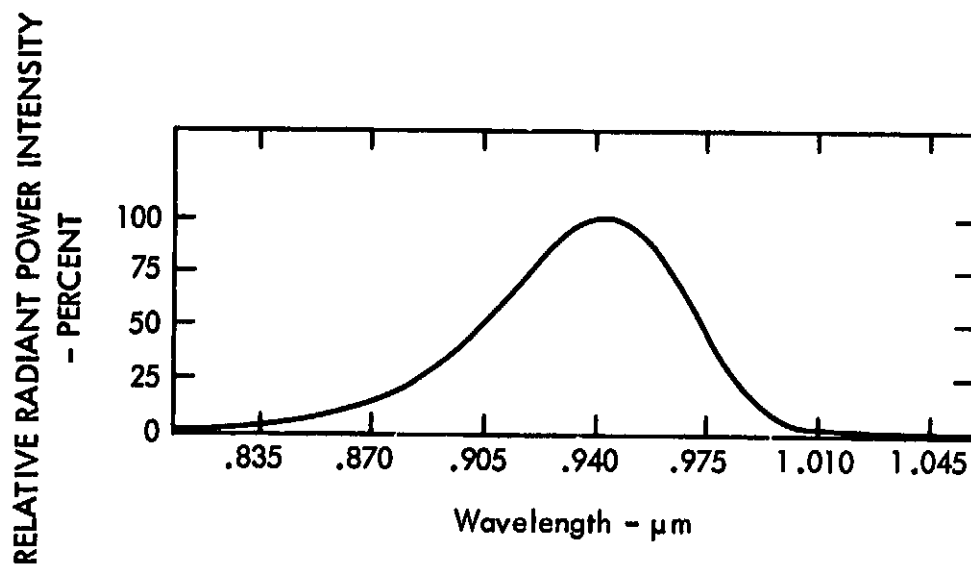


Figure 6. Spectral Response Curve For The TIL-31 Light Emitting Diode

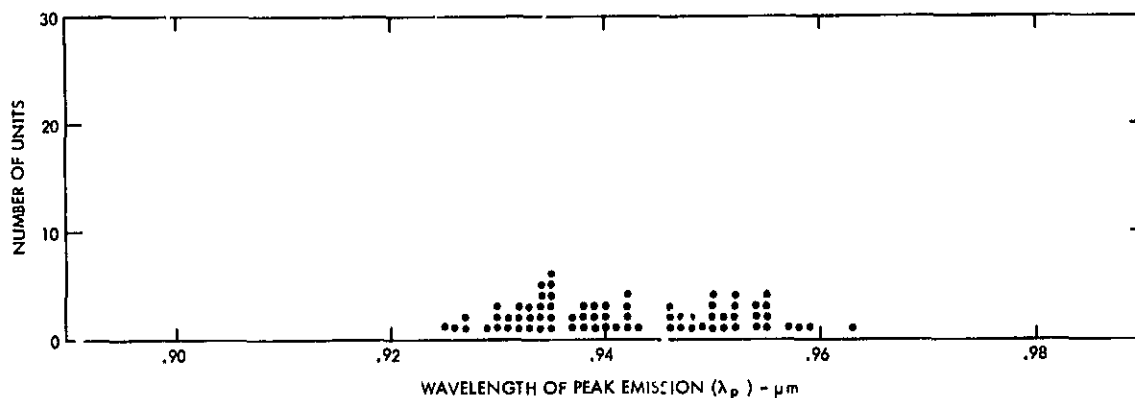


Figure 7 (a) Distribution Of Initial Values Of Wavelength Of Peak Emission ( $\lambda_p$ ) Measured At 100 mA.

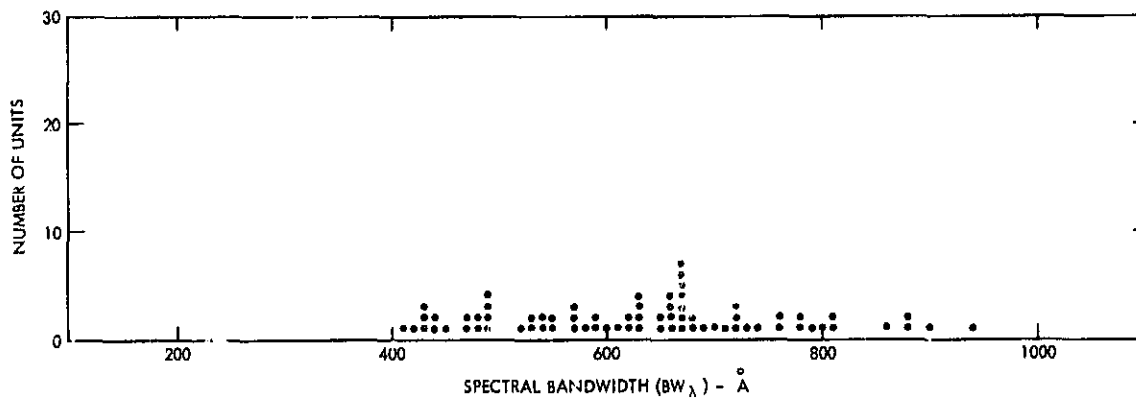


Figure 7 (b) Distribution Of Initial Values Of Spectral Bandwidth ( $BW_\lambda$ ) Measured At 100 mA.

Figure 7. Initial Values Of  $\lambda_p$  And  $BW_\lambda$  For The TIL-31

ORIGINAL PAGE IS  
OF POOR QUALITY

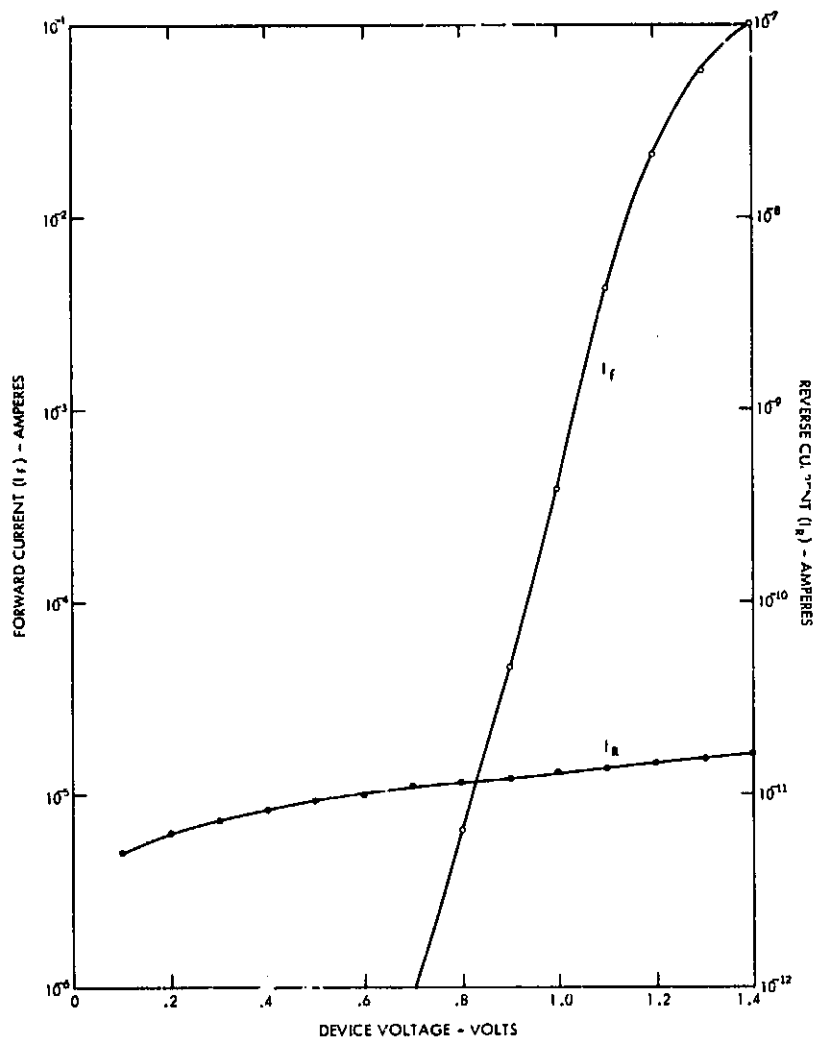


Figure 8. Typical I-V Characteristic Curves For The TIL-31

ORIGINAL PAGE IS  
OF POOR QUALITY

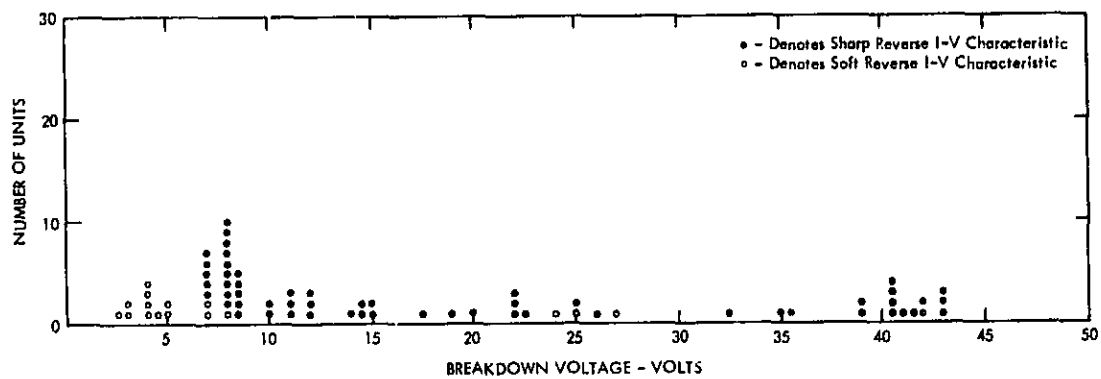


Figure 9. A Distribution Of Initial Reverse Breakdown Voltage Values Measured At 10  $\mu$ A

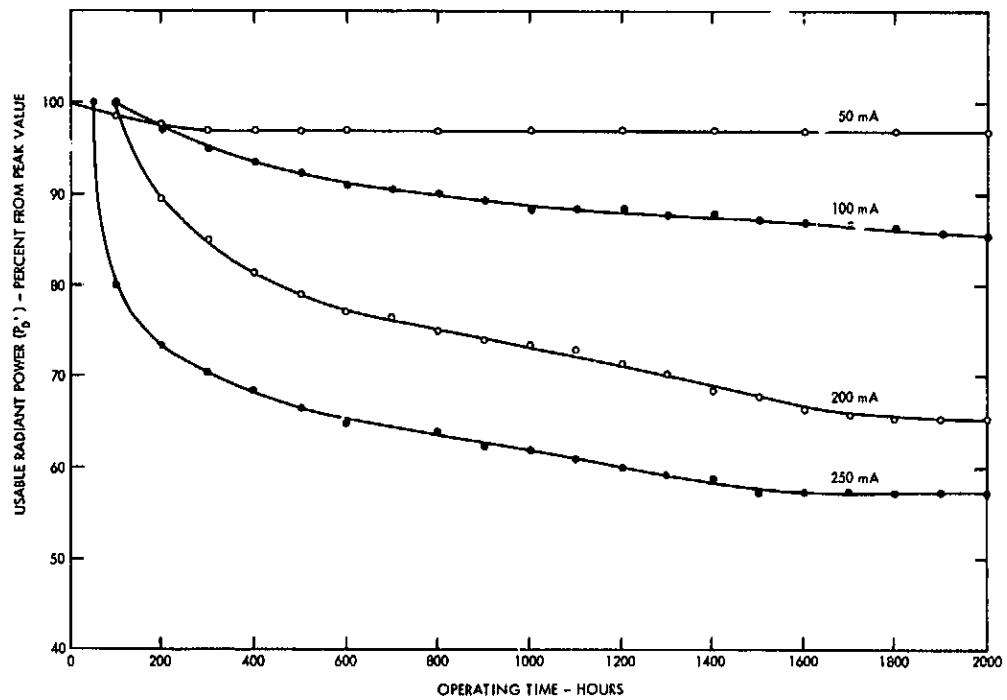


Figure 10. Usable Radiant Power ( $P_0'$ ) As A Function Of Current Stress And Operating Time For An Ambient Temperature of 298K

ORIGINAL PAGE IS  
OF POOR QUALITY



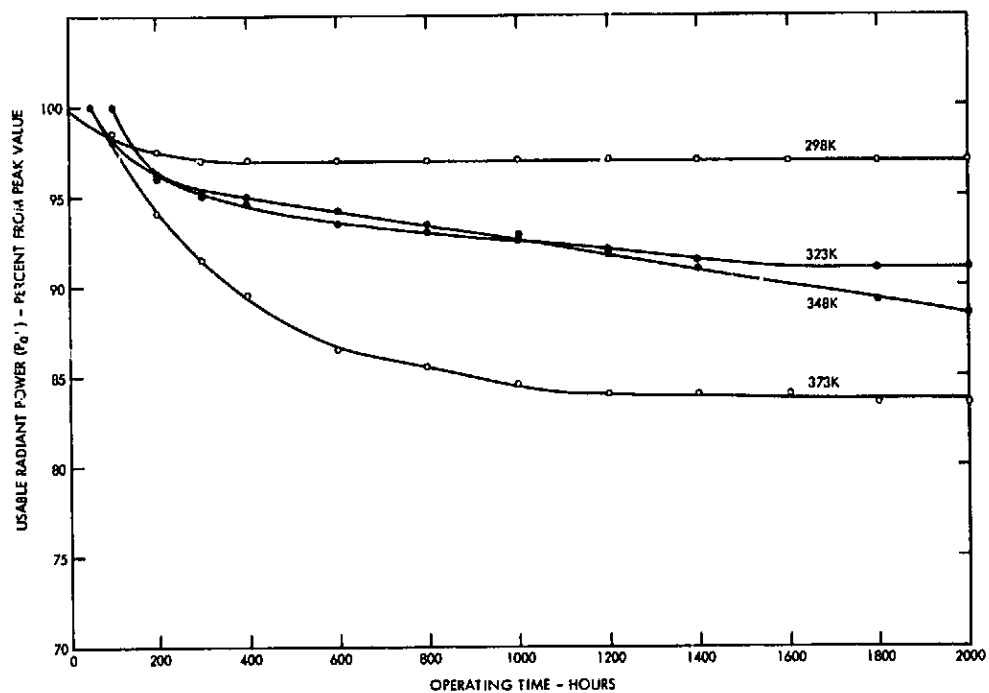


Figure 11. Usable Radiant Power ( $P_0$ ) As A Function Of Ambient Temperature And Operating Time For A Current Stress Of 50 Milliamperes

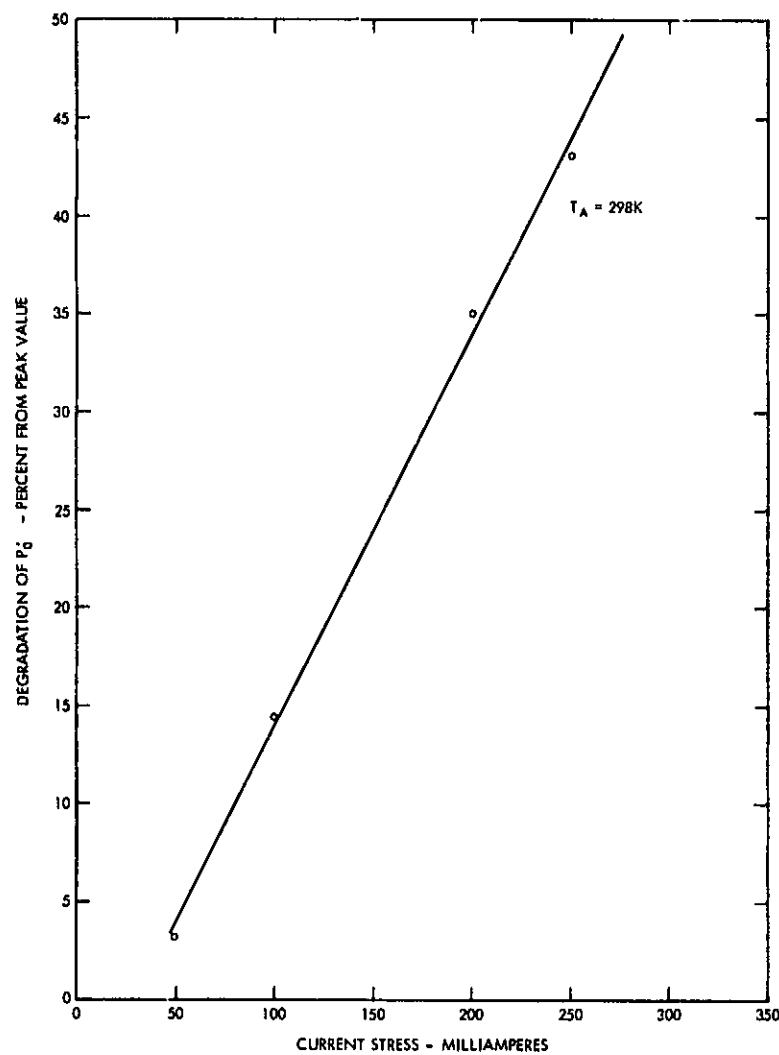


Figure 12 (a) A Plot Of The Degradation of  $P_0$  As A Function Of Current Stress After Two Thousand Hours Of Operation At An Ambient Temperature of 298K

ORIGINAL PAGE IS  
OF POOR QUALITY

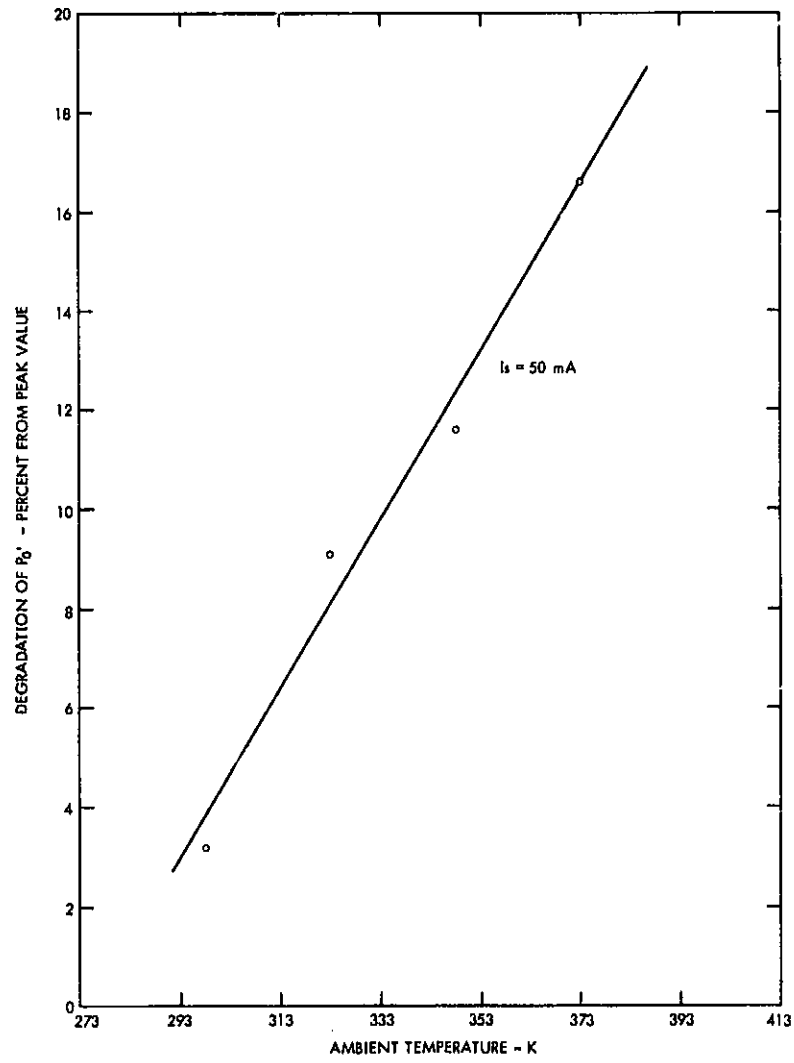


Figure 12 (b) A Plot Of The Degradation Of  $P_0'$  As A Function Of Ambient Temperature After Two Thousand Hours Of Operation At A Current Stress Of 50 Milliampères

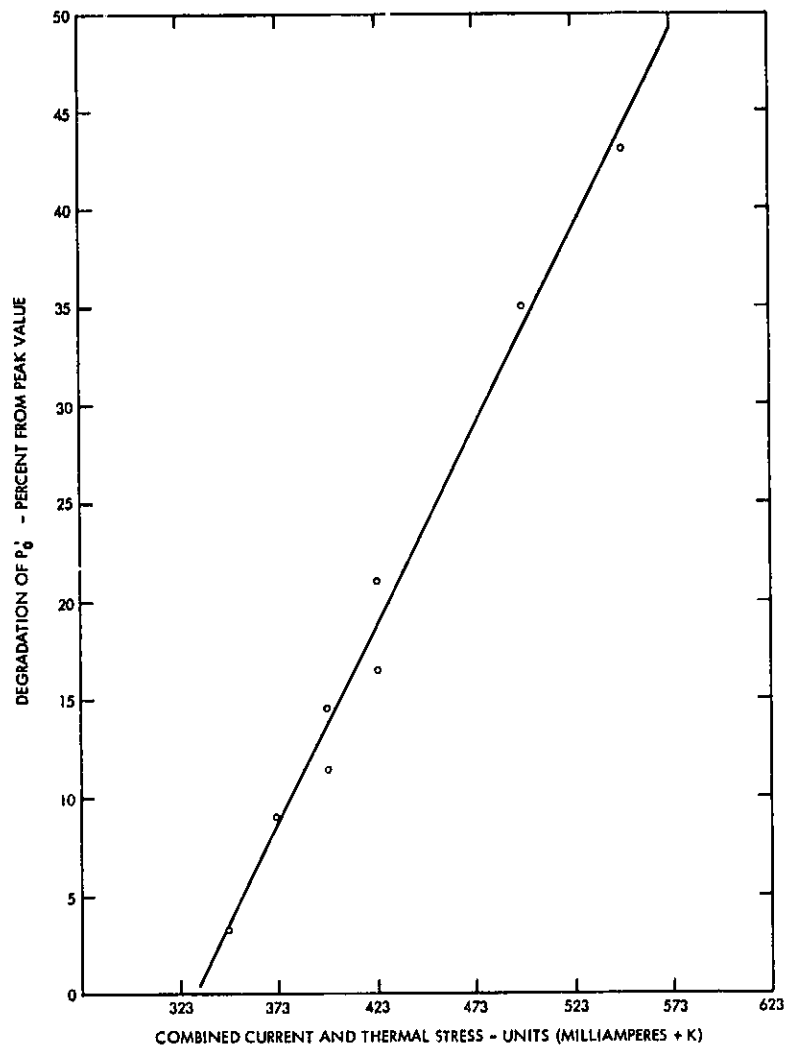


Figure 12 (c) A Plot Of The Degradation Of  $P_0'$  As A Function Of The Combined Stress Variables Of Current And Temperature After Two Thousand Hours Of Operation

ORIGINAL PAGE IS  
OF POOR QUALITY

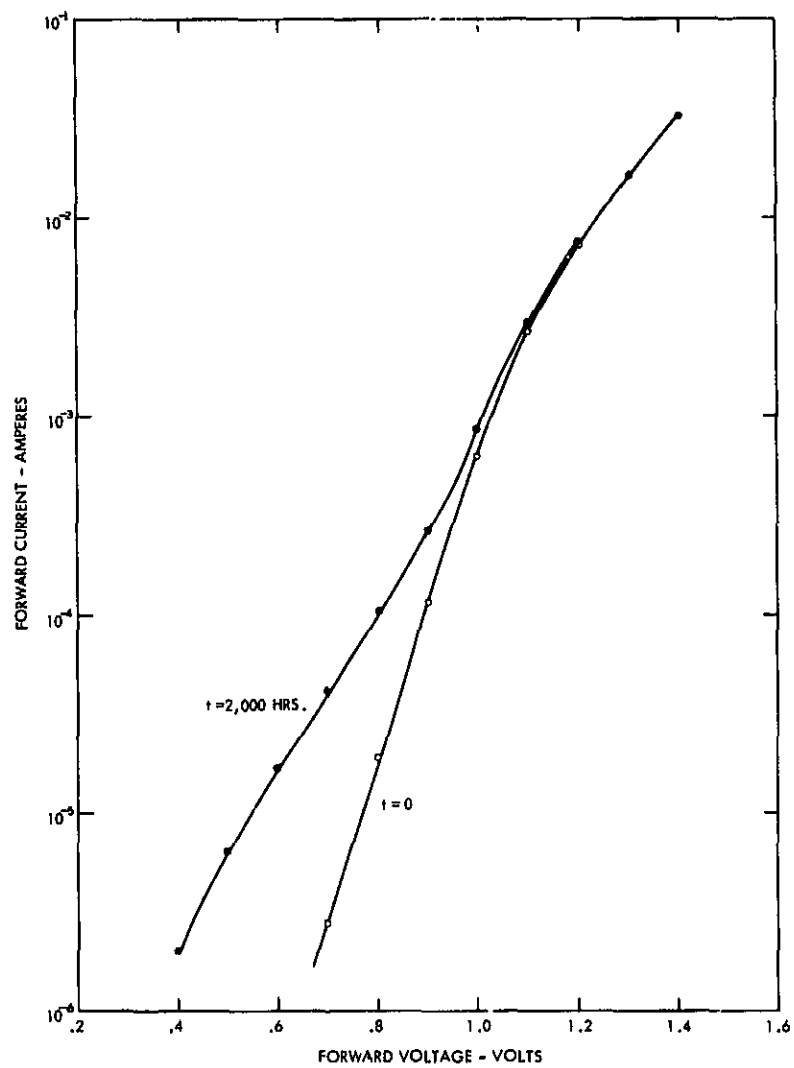


Figure 13 Typical Change In The Forward I-V Characteristics After Two Thousand Hours Of Operation At A Current Stress Of 250 Milliamperes And An Ambient Temperature Of 298K

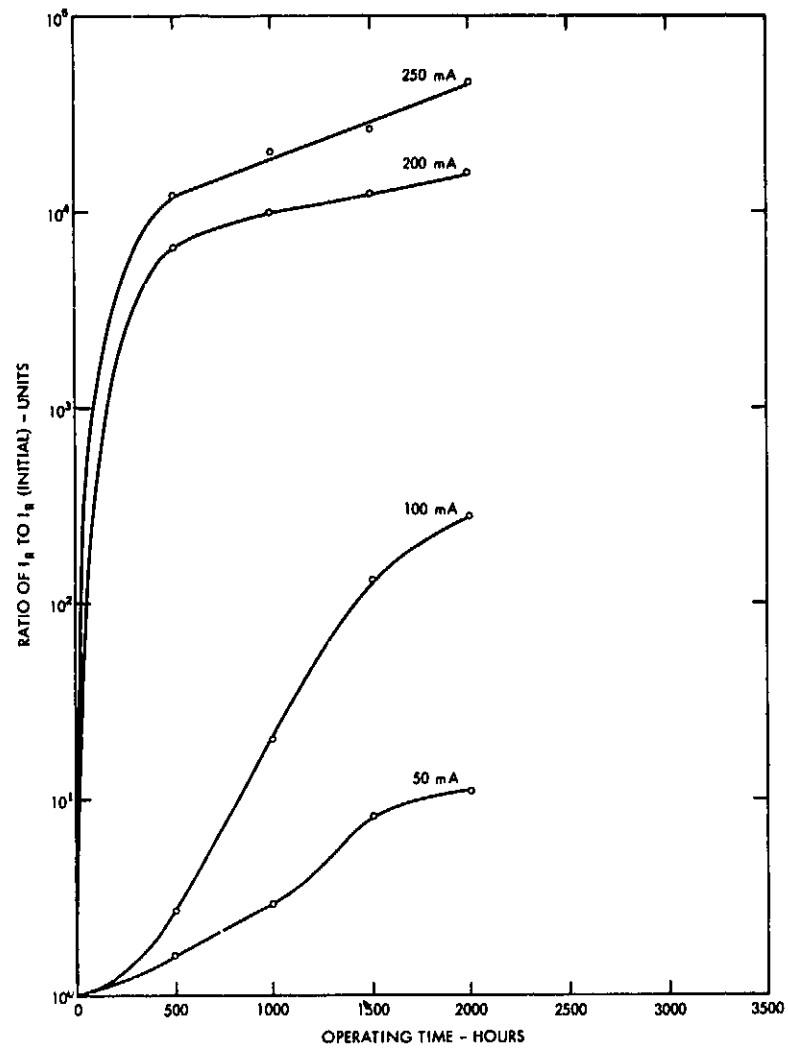


Figure 14 A Plot of the Change in the Reverse Leakage Current as a Function of Current Stress and Operating Time at an Ambient Temperature of 298K

ORIGINAL PAGE IS  
OF POOR QUALITY

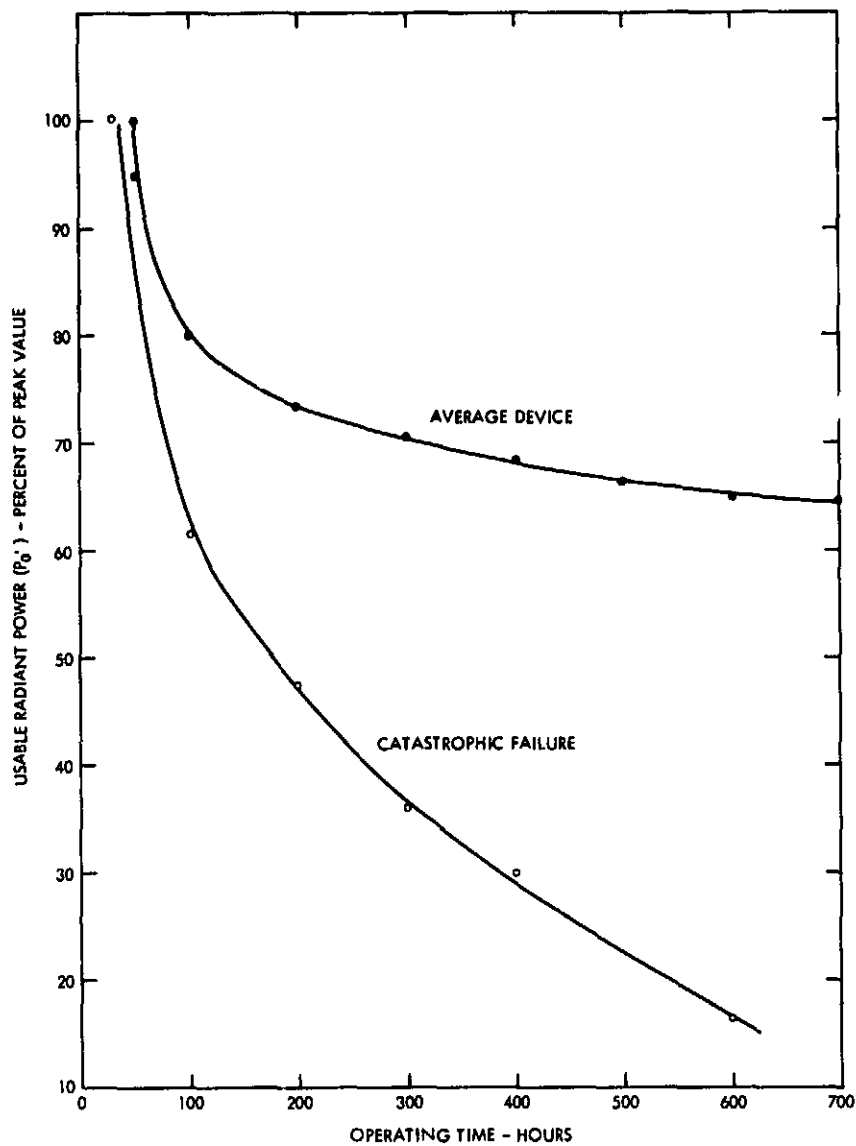


Figure 15 A Comparison Of The Degradation Of  $P_0'$  For The Catastrophically Failed Device And The Average Device Operated At A Current Stress Of 250 Milliamperes And An Ambient Temperature of 298K

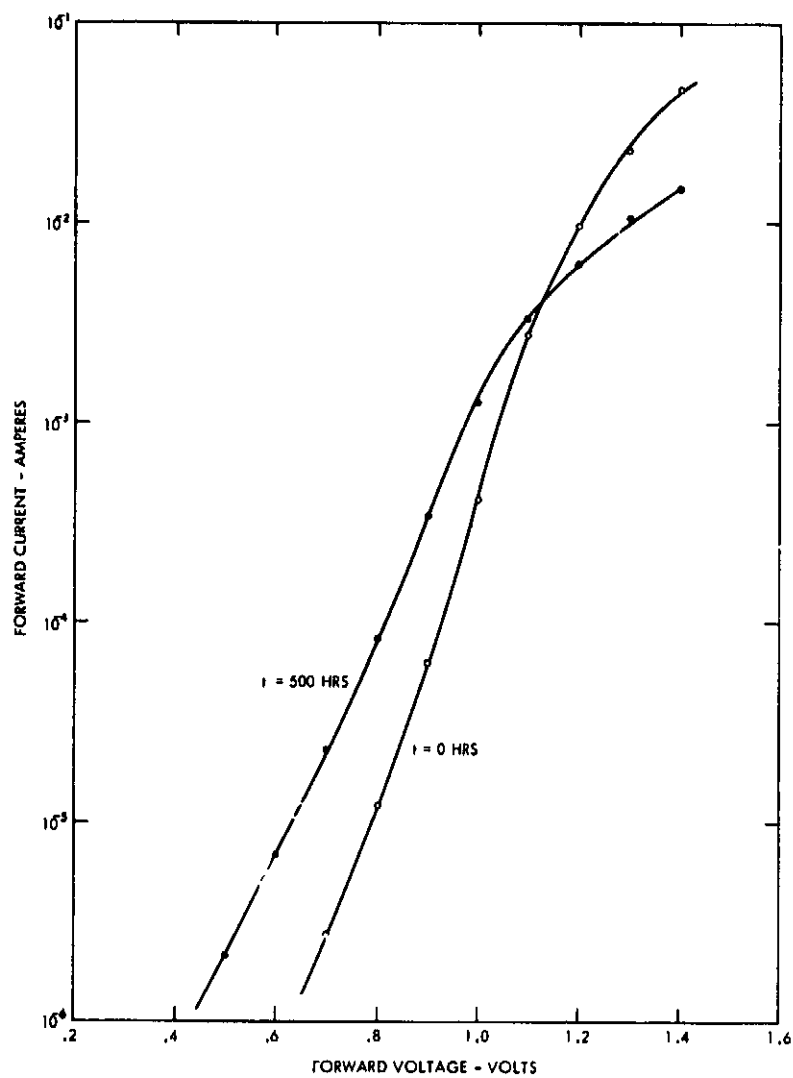


Figure 16 Degradation In The Forward I-V Characteristics For The Catastrophically Failed Device

ORIGINAL PAGE IS  
OF POOR QUALITY



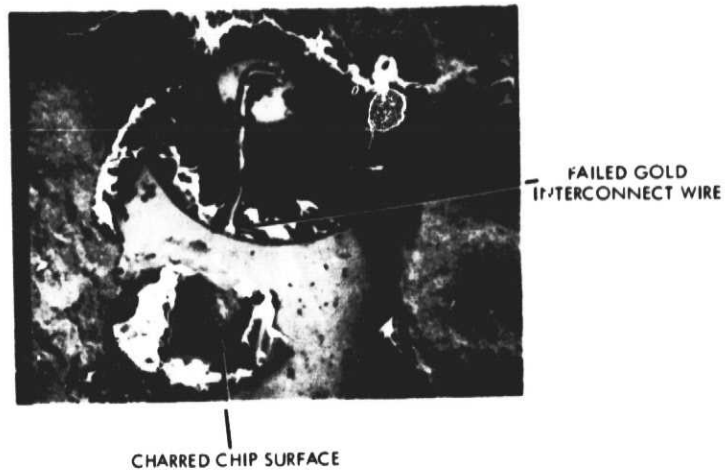


Figure 17 SEM Photograph Of The Catastrophically Failed Device  
Showing The Damaged Chip And Internal Lead Wire (50 X. MAG)

ORIGINAL PAGE IS  
OF POOR QUALITY

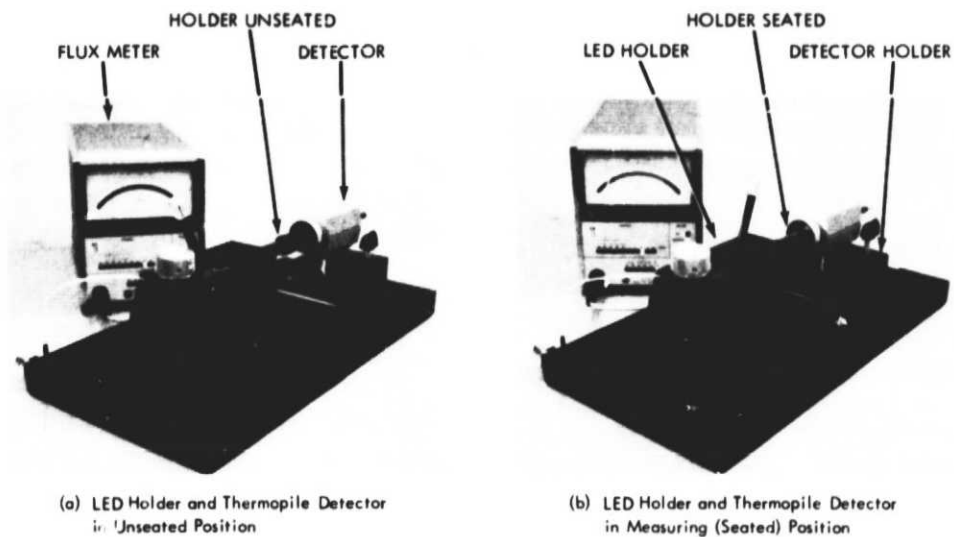


Figure 18. Test Configuration For Measuring Usable Radiant Power Output Of The TIL-31 Infrared LED.

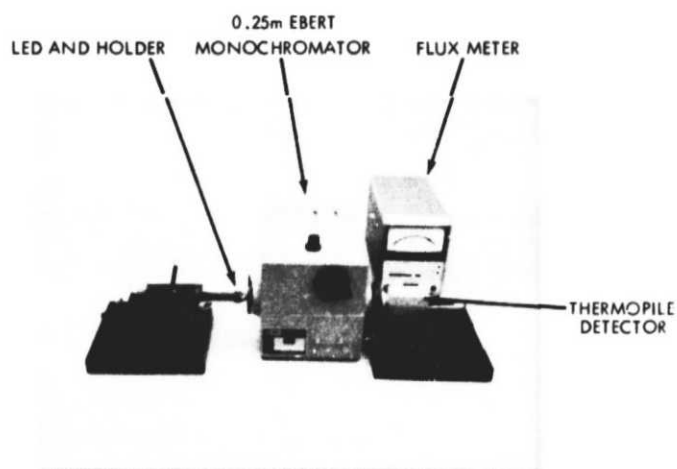


Figure 19 Test Configuration For The Wavelength Of Peak Emission ( $\lambda_p$ ) And Spectral Bandwidth ( $BW_\lambda$ ) Measurements

ORIGINAL PAGE IS  
OF POOR QUALITY

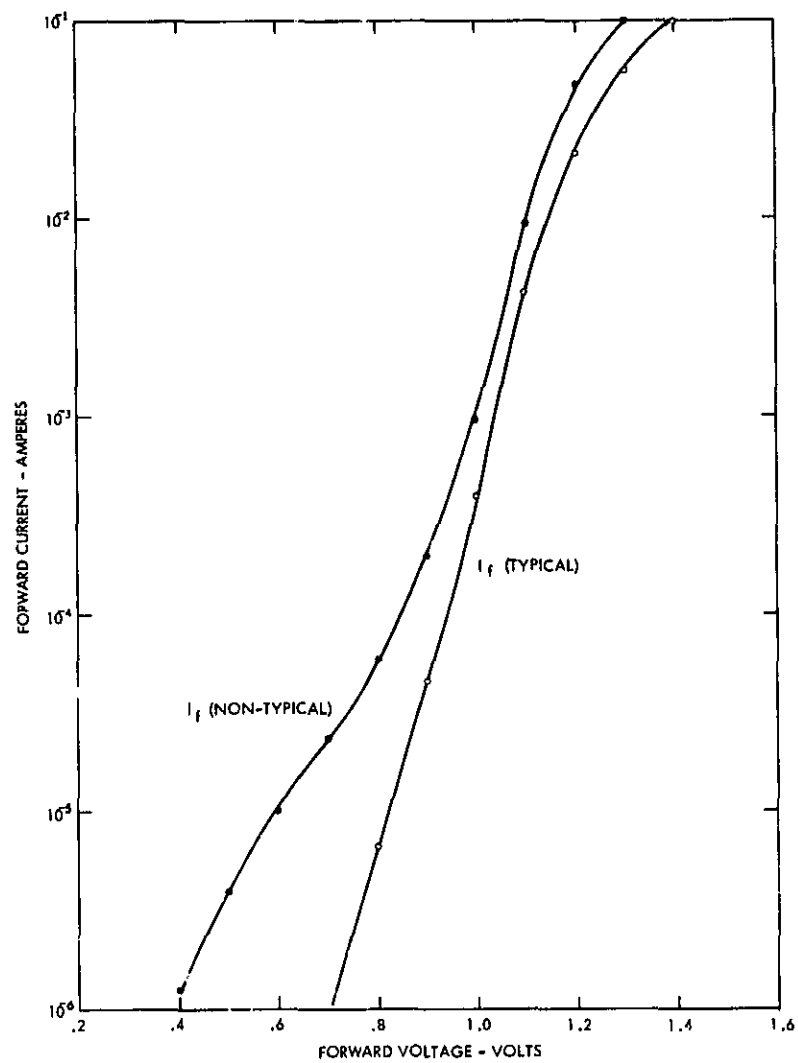


Figure 20 (a) Examples Of Typical And Non-Typical Forward I-V Characteristics For The TIL-31

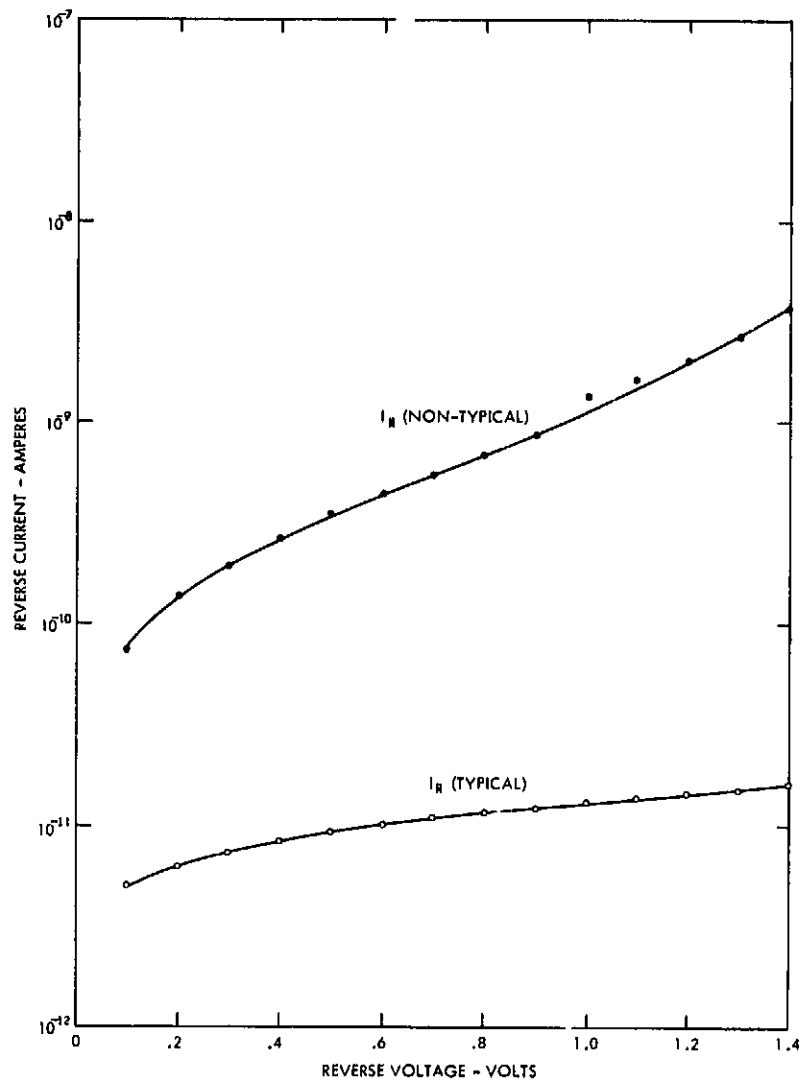


Figure 20 (b) Examples Of Typical And Non-Typical Reverse I-V Characteristics For The TIL-31

ORIGINAL PAGE IS  
OF POOR QUALITY